Inorganic Chemistry

Article

pubs.acs.org/IC

Organometallic Iridium Complex Containing a Dianionic, Tridentate, Mixed Organic–Inorganic Ligand

Aaron J. Bloomfield, Adam J. Matula, Brandon Q. Mercado, Victor S. Batista, and Robert H. Crabtree*

Department of Chemistry, Yale University, 225 Prospect Street, New Haven, Connecticut 06520, United States

Supporting Information

ABSTRACT: A pentamethylcyclopentadienyl–iridium complex containing a tricyclic, dianionic, tridentate, scorpionate (facial binding), mixed organic–inorganic ligand was synthesized and characterized by single-crystal X-ray crystallography, as well as polynuclear NMR, UV–vis, and IR spectroscopies. The central cycle of the tridentate ligand consists of a modified boroxine in which two of the boron centers are tetrahedral, anionic borates. The complex is stable to hydrolysis in aqueous solution for >9 weeks at 25 °C but reacts with a 50 mM solution of sodium periodate within 12 s to form a periodate-driven oxygen evolution catalyst that has a turnover frquency of >15 s^{-1}. However, the catalyst is almost completely deactivated within 5 min, achieving an average turnover number of ca. 2500 molecules of oxygen per atom of iridium. Nanoparticles were not observed on this time scale but did form within 4 h of catalyst activation under these experimental conditions. The parent complex was modeled using density functional theory, which accurately reflected the geometry of the complex and indicated significant interaction of iridium- and boracycle-centered orbitals.

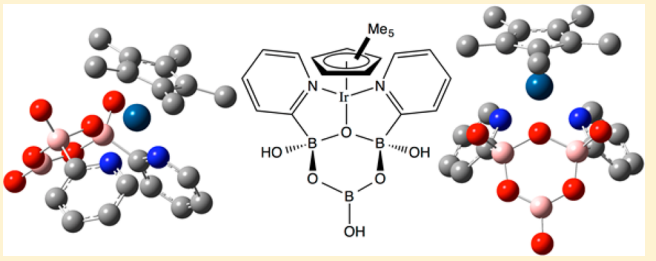

INTRODUCTION

Several organometallic half-sandwich complexes of iridium containing pentamethylcyclopentadienyl (Cp*) and chelating polydentate ligands have been shown to be active catalysts or precursors of catalysts for oxygen evolution,[1−11] oxygen reduction,[12] C–H bond functionalization,[11,13−15] and transfer hydrogenation.[12,16] Complexes with neutral bidentate ligands (Chart 1), such as **1a** and **1b**, are competent oxygen evolution precatalysts when using sodium periodate[1,3,4] or ceric ammonium nitrate (CAN)[9] as the terminal oxidant, while **1c** has been shown to be catalytically inert.[1] Monoanionic bidentate N,C (**2a**–**2c**)[4,7−9] and N,O (**3a**–**3c**)[1−6] ligands have also been shown to be active for oxygen evolution using either chemical or electrochemical[5] oxidants. Of these, complex **3a**, containing the chelating pyridine alkoxide ligand "pyalc", forms a particularly active oxygen evolution[1−6,11] and C–H activation[11,13−15] catalyst. Complexes containing dianionic chelating ligands have also been demonstrated as competent for oxygen evolution (**4a**),[10] oxygen reduction (**4b**),[12] and transfer hydrogenation (**4b** and **4c**).[12,16]

The relative activity of the N,O-ligand-containing complexes (**3a** > **3b** > **3c**) demonstrated by Koelewijn et al.[6] follows the trend of both the donor power and pK_a of the oxygen terminus of the ligand, where more basic, more donating ligands generate more active catalysts. In an effort to investigate these trends more thoroughly, complex **5** was targeted because the pK_a of the borate is expected to be between that of the carboxylate and sulfonate,[17] while the donating power might be expected to be reduced as the formally anionic center is farther removed from the iridium atom (Figure 1). Additionally, the trihydroxyborate might be capable of several potentially interesting hydrogen-bonding interactions with substrates.

Although the instability of pyridine-2-boronic acid and its corresponding lithium borate salt under protic conditions has been reported as highly problematic,[18,19] other researchers have since successfully isolated the lithium salt.[20] Therefore, sodium trihydroxy(2-pyridyl)borate (Na-Pybor, **6**; Scheme 1) was targeted as a viable precursor of **5**. The preparation of **6** from the commercially available dimethylboronate ester and sodium hydroxide (prepared in situ by hydrolysis of sodium *tert*-butoxide) proceeded quantitatively in water.

6 was found to be effectively stable in a mildly alkaline aqueous solution for several hours at 23 °C. A solution of **6** in D_2O was found to decompose to 2-deuteropyridine with a half-life of about 1 week (Figure S6). However, the reaction of **6** with $(Cp^*IrCl_2)_2$ in water resulted in the formation of multiple iridium- and boron-containing compounds, including complex **7**, which selectively crystallized out of the worked-up reaction mixture and contains an unexpected, dianionic, tridentate, boracycle-containing ligand (Dipytribor).

The class of boron-containing anions contains a particularly rich variety of structures, but there have only been a small number of reports of molecular transition-metal[21−30] or main-group metal[31] complexes paired with partially organic or completely inorganic polyborate counterions and fewer reports of the borate anions serving as monodentate,[25,30] bidentate,[27,31] or tridentate[27] ligands, coordinating to the metal through

Received: May 18, 2016

DOI: 10.1021/acs.inorgchem.6b01218
Inorg. Chem. XXXX, XXX, XXX–XXX

Chart 1. Relevant Cp*Ir^{III} Half-Sandwich Complexes Containing Chelating Ligands

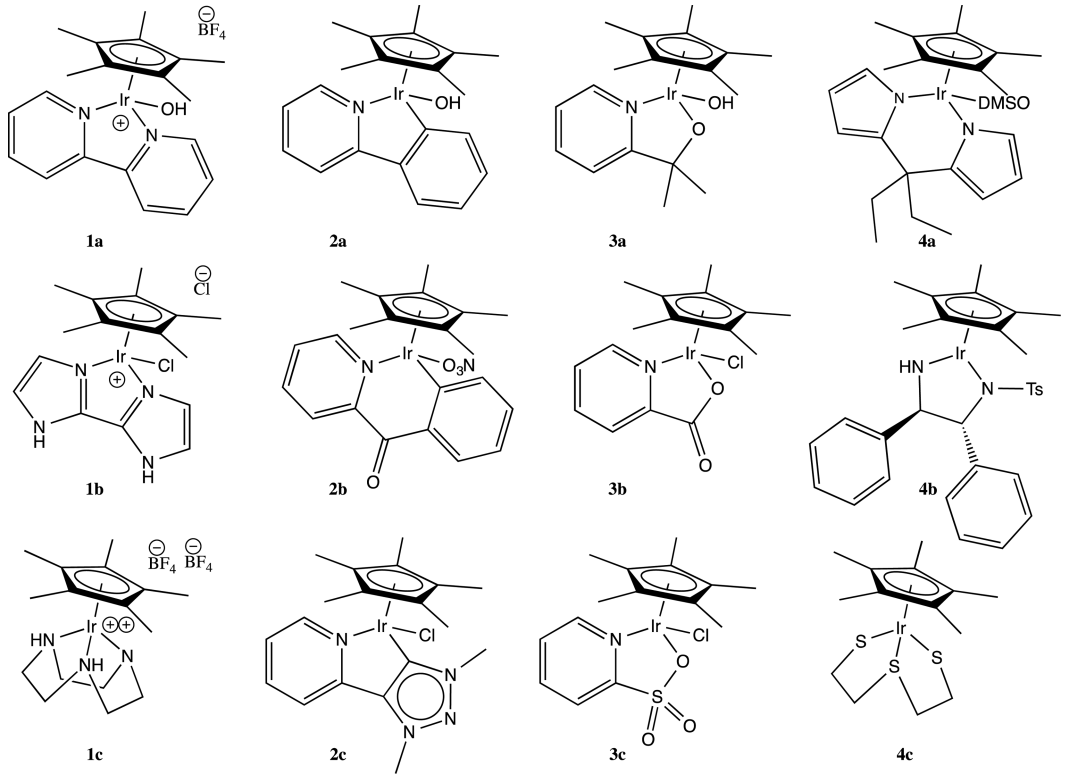

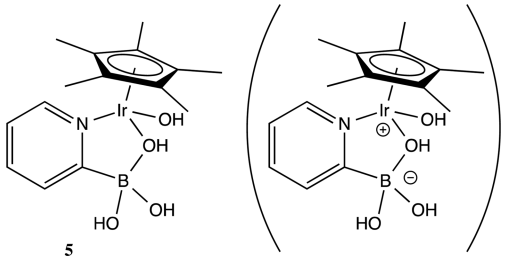

Figure 1. (Left) Targeted Cp*Ir(OH)Pybor complex (**5**). (Right) Formally zwitterionic representation.

oxygen atoms. There have also been reports of such anions accompanying organic cations.[32−34]

Polydentate organoboron ligands containing a tetrahedral, anionic boron atom in the backbone are a common and useful class, including tridentate scorpionate ligands, like tris(pyrazolyl)borate.[35−37] In some cases, the boron center within the ligand is activated, and one of the substituents is replaced by the bound metal center, resulting in a metallaboratrane complex.[38−41] There is also at least one report of cleavage of a B−aryl bond during metalation of diphenylbis(pyrazolyl)borate.[42]

Herein we report the synthesis and characterization of an organometallic iridium complex with a boron-containing ligand and examine the application of this complex to oxygen evolution catalysis.

EXPERIMENTAL SECTION

Synthesis of Sodium Trihydroxy(2-pyridyl)borate (Na-Pybor, 6). Dimethyl (2-pyridyl)boronate (383 mg, 2.25 mmol, 1 equiv) and sodium *tert*-butoxide (275 mg, 2.86 mmol, 1.27 equiv) were combined in a 5-dram vial, open to air. Deionized water (6.0 mL) was added, and the mixture was sonicated for 60 s. The resulting homogeneous solution was then heated to 35 °C and evaporated to dryness over the course of 25 min using a dynamic vacuum and a carbon dioxide/acetone cold solvent trap. The resulting white solid (430 mg, quant.) was a single organoboron species (27 mol % excess sodium hydroxide) and was used without further purification.

^{1}H NMR (400 MHz, D_2O): δ 8.46 (d, J_{HH} = 5.2 Hz, 1H, H1), 7.71 (dt, J_{HH} = 7.6 and 2.0 Hz, 1H, H4), 7.61 (d, J_{HH} = 7.6 Hz, 1H, H3), 7.23 (t, J_{HH} = 6.4 Hz, 1H, H2). ^{11}B NMR (160 MHz, D_2O): δ 1.5. ^{13}C NMR (150 MHz, D_2O): δ 175.6 (C5), 146.7 (C1), 135.8 (C4), 126.0 (C3), 121.1 (C2). IR (diamond, thin film): 3626 (w), 3367 (br), 3037

Scheme 1. Synthesis of 6 and Transformation in Complex 7

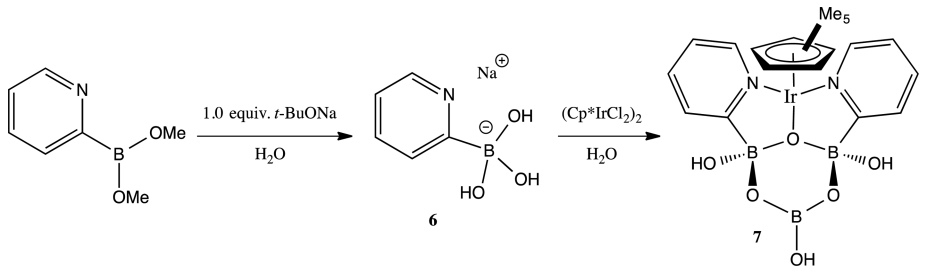

DOI: 10.1021/acs.inorgchem.6b01218
Inorg. Chem. XXXX, XXX, XXX−XXX

(w), 2999 (w), 1587 (m), 1555 (w), 1421 (m), 1272 (m), 1152 (m), 1094 (m), 1049 (m), 958 (s), 908 (s), 856 (s), 770 (s), 742 (s), 629 (s), 607 (s) cm^{-1}.

Synthesis of Pentamethylcyclopentadienyliridium(III) *meso*-2,4,6-Trihydroxy-2,4,-di(2-pyridyl)-1,3,5,2,4,6-trioxaborinane-2,4-diuide (Cp*IrDipytribor, 7). **6** (121 mg, 629 μmol of Pybor, 1 equiv) was dissolved in deionized water (2.0 mL). Then powdered $(Cp^*IrCl_2)_2$ (238 mg, 597 μmol of iridium, 0.95 equiv; prepared by the method of Tönnemann et al.[43]) was added, and the resulting suspension was mixed and sonicated at 25 °C until a pale-orange homogeneous solution was obtained (ca. 35 min). The resulting solution was diluted with deionized water (2 × 10 mL) and transferred to a 150 mL separatory funnel. The aqueous layer was washed with two portions of dichloromethane (25 mL) and then extracted three times with a 3:1 (w/w) mixture of dichloromethane and *tert*-butyl alcohol (3 × 50 mL). The alcoholic extracts were combined, evaporated to dryness, and then dissolved in a 1:1 (w/w) mixture of *tert*-butyl alcohol and ethyl acetate (ca. 10 mL). The resulting solution was filtered into a 5-dram vial, and an equal volume of hexanes was layered on top. Analytically pure 7 was obtained as pale-yellow prismatic crystals.

^{1}H NMR (500 MHz, D_2O): δ 8.53 (d, J_{HH} = 5.0 Hz, 2H, H1), 7.54 (dt, J_{HH} = 7.75 and 1.15 Hz, 2H, H3), 7.26 (d, J_{HH} = 7.5 Hz, 2H, H4), 7.11 (dt, J_{HH} = 6.75 and 1.5 Hz, 2H, H2), 1.49 (s, 15H, Cp* Me). ^{11}B NMR (160 MHz, D_2O): δ 19.3, 5.6. ^{13}C NMR (125 MHz, D_2O): δ 178.6 (C5), 148.8 (C1), 136.9 (C3), 127.5 (C4), 124.6 (C2), 87.1 (Cp* ring), 8.0 (Cp* Me). IR (diamond, thin film): 3411.8 (br), 2917 (w), 2496 (br), 1600 (m), 1447 (m), 1383 (s), 1332 (s), 1204 (m), 1090 (m), 1004 (s), 884 (s), 766 (s), 680 (s) cm^{-1}.

Single-Crystal Structure Determination of 7. Low-temperature diffraction data (ω scans) were collected on a Rigaku MicroMax-007HF diffractometer coupled to a Saturn994+ CCD detector with Cu Kα (λ = 1.54178 Å) for the structure of 7. The diffraction images were processed and scaled using the Rigaku Oxford Diffraction software.[44] The structure was solved with *SHELXT* and refined against F^2 on all data by full-matrix least squares with *SHELXL*.[45] All non-hydrogen atoms were refined anisotropically. Hydrogen atoms were included in the model at geometrically calculated positions and refined using a riding model. The isotropic displacement parameters of all hydrogen atoms were fixed to 1.2 times the *U* value of the atoms to which they are linked (1.5 times for methyl groups). The only exception is the hydrogen atoms associated with oxygen atoms. These positions were found in the difference map, but free refinement presented unreasonable O−H distances. The distances were subsequently fixed to values of 0.950 (0.002) Å, and the positional parameters were freely refined. The full numbering scheme of compound 7 can be found in the full details of the X-ray structure determination (CIF), which is included as Supporting Information.

Density Functional Theory (DFT) Calculations. DFT calculations were carried out using *Gaussian 09*. Gas-phase enthalpies were calculated at the B3LYP/DEF2SVP level using minimum-energy structures obtained at the same level of theory.

RESULTS AND DISCUSSION

Solution-phase NMR of 7 in D_2O at 23 °C (Table 1 and Figures S7−S11) indicates a high degree of symmetry, in which both pyridyl rings are equivalent (by ^{1}H and ^{13}C NMR), and there are only two distinct boron chemical environments (by ^{11}B NMR): one at 5.6 ppm, assigned as tetrahedral, and one at 19.3 ppm, assigned as trigonal. The Cp* ring is also freely rotating under these conditions, showing only one sharp singlet in the ^{1}H NMR spectrum and two signals in the ^{13}C NMR spectrum (endocyclic and exocyclic carbon atoms).

In the crystal, however, this symmetry is broken by the orientation of the hydroxyl group bound to the trigonal boron center. The unit cell contains two crystallographically inequivalent molecules of each configuration. Parts A and B of Figure 2 show one of these molecules from two perspectives.

Table 1. Details of X-ray Crystal Structure 7

compound	Cp*IrDipytribor (7)
empirical formula	$C_{20}H_{30}B_3IrN_2O_8$
fw	651.09
cryst syst	monoclinic
space group	$P2_1/n$
a (Å)	9.3069(2)
b (Å)	16.4356(3)
c (Å)	15.5445(3)
α (deg)	90
β (deg)	100.959(2)
γ (deg)	90
V (Å^3)	2334.39(8)
Z	4
ρ(calcd) (g cm^{-3})	1.853
μ (mm^{-1})	11.501
R1, wR2 [$I > 2\sigma(I)$]	0.0386, 0.1016
R1, wR2 (all data)	0.0452, 0.1066
GOF	1.057

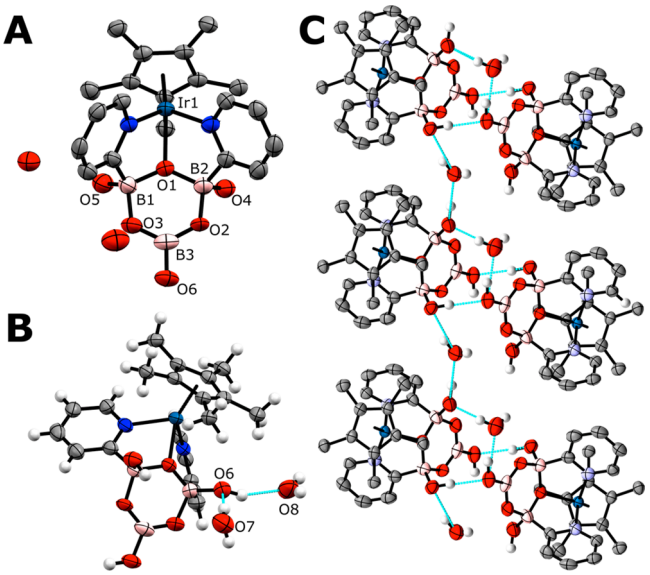

Figure 2. Thermal ellipsoid representation of the crystal structure of 7 at the 50% level (some hydrogen atoms are excluded for clarity; any shown are depicted as arbitrary spheres). A and B show two views of one molecule of 7 with two associated water molecules, while C shows a view of the hydrogen-bonding network along the *a* axis (hydrogen bonds tabulated in Table S7).

Additionally, the unit cell contains interstitial water molecules that are hydrogen-bound to the hydroxyl substituents on the boracycle in an unsymmetrical fashion. Together the inorganic rings and water molecules have self-assembled to create parallel channels of hydrogen-bonded species that run through the entire crystal. Figure 2C shows multiple adjacent molecules, highlighting the hydrogen-bonding network.

The Ir−O bond in 7 was found to be only 2.092(3) Å. Of the 31 iridium ether complexes with reported crystal structures (average Ir−O bond length of 2.218 Å), only five contain Ir−O bonds shorter than 2.13 Å, all of which are monocationic iridium(I) complexes,[46−48] and of these, only two have shorter Ir−O bonds than those observed for 7 (SAHYEG[46] and QUKLIR[47]). For three of these five compounds, the ether in question is part of a neutral, bidentate, N,O-chelating ligand that forms a five-membered metallacycle. Thus, it is perhaps

DOI: 10.1021/acs.inorgchem.6b01218
Inorg. Chem. XXXX, XXX, XXX−XXX

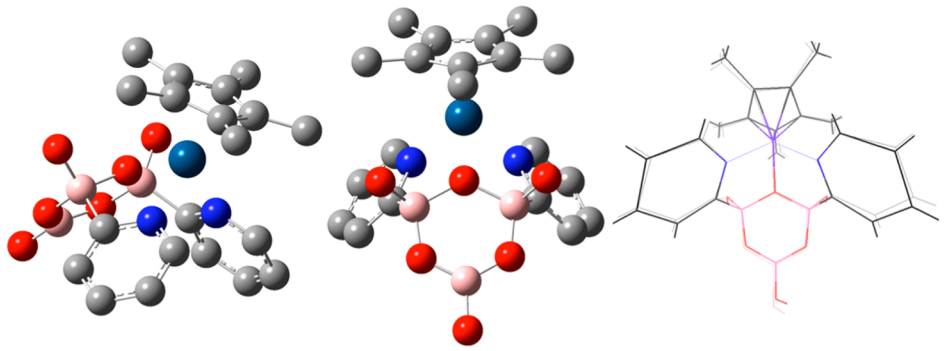

Figure 3. Computed structure of **7** viewed from two angles and overlaid with its crystal structure.

Table 2. Calculated Enthalpies of Reaction and Bond Lengths of Hypothetical Analogues

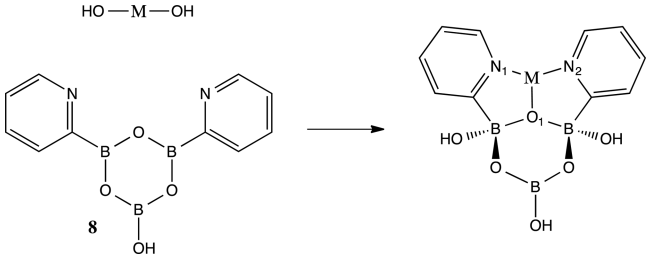

M	ΔH (kcal mol^{-1})	O_1–M (Å)	N_1–M (Å)	N_2–M (Å)	B–O_1 (Å)
Cp*Ir	−65.77	2.08	2.11	2.11	1.52
d^0 metals					
Ca	−44.86[a]	2.09	2.37	2.46	1.50
Sr	−52.79[a]	2.23	2.55	2.63	1.49
Ba	−76.17[b]	2.54	2.91	2.94	1.46
Cp*Y	−43.16	2.15	2.40	2.50	1.51
Cp*La	−43.79	2.30	2.59	2.69	1.49
d^{10} metals					
Zn	−51.03	1.89	1.96	1.96	1.52
Cd	−38.87	2.14	2.16	2.16	1.49
Hg	−25.58	2.28	2.12	2.12	1.48

[a]Bonding to one exocyclic oxygen atom. [b]Bonding to both exocyclic oxygen atoms.

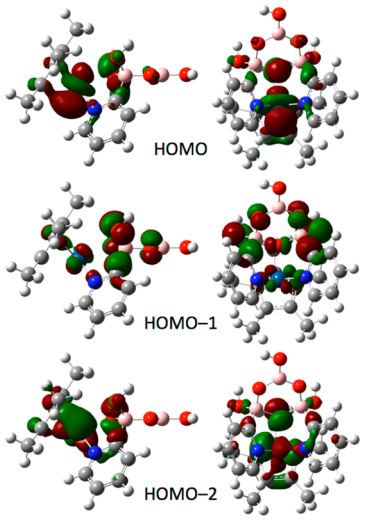

Figure 4. Visualizations of the three HOMOs, each viewed from two angles.

unsurprising that the doubly anionic, doubly chelated, tridentate ligand bound to a formally dicationic iridium center has such a short Ir–O contact.

Interestingly, the boracycle in **7** is hydrolytically robust, showing no sign of decomposition or interconversion by ^{1}H or ^{11}B NMR over the course of 9 weeks as a dilute solution (<10 mM) in unbuffered water (D_2O) at 23 °C. In addition to being less susceptible to protonolysis than **6** is, this indicates a stark contrast to most reported neutral boroxines, which undergo very facile hydrolysis.[49] One study reported complete hydrolysis of an aryl-substituted boroxine in 4% water/acetonitrile within 10 s.[50] Anionic borate oligomers (both cyclic and acylic) are also subject to hydrolysis. Studies of the speciation of borate anions in aqueous solution indicate that, at 25 °C, solutions of $Li_2B_4O_7$ (at total boron concentrations of up to 750 mM) contain almost entirely $B(OH)_3$ and $B(OH)_4^-$, with traces of $B_3O_3(OH)_4^-$.[51] Only with concentrations approaching and exceeding 1 M were significant concentrations of higher oligomers detected. Similarly, solutions prepared by the dissolution of sodium and potassium polyborates in water were observed to contain mostly $B(OH)_3$ and $B(OH)_4^-$, with $B_3O_3(OH)_4^-$ and higher oligomers accounting for less than one-third of the total boron content when prepared from $KB_5O_8{\cdot}4H_2O$ or $NaB_5O_8{\cdot}5H_2O$ with boron concentrations between 50 and 150 mM.[52] With more basic salts like $K_2B_5O_8(OH){\cdot}2H_2O$, the species were reported to undergo rapid exchange.

It is also unclear how the boracycle in **7** formed in the first place. As mentioned in the Introduction, both pyridine-2-boronic acid and its lithium borate salt have been reported as unstable in protic solvents.[18−20] In our hands, **6** appears to be relatively stable in aqueous solution, decomposing with a half-life of about 1 week, but reacts quickly with $(Cp^*IrCl_2)_2$ to form a mixture of at least four Cp*Ir-containing complexes (as seen by ^{1}H NMR) and at least three chemically inequivalent boron species (as seen by ^{11}B NMR). Given the propensity of iridium to activate B–H bonds[38] and the report of the rhodium-mediated cleavage of a B–C bond in a rhodium(III) complex of an aryl borate,[42] it is not unreasonable to suspect that an iridium species in the reaction mixture may promote scission of the B–C bond in **6**.

The gas-phase DFT-optimized structure of **7** (Figure 3) was obtained using the hybrid B3LYP exchange-correlation functional and the def2svp basis set with unrestricted Kohn–Sham wave functions, as implemented in the *Gaussian 09* package.[53] Favorable comparison of the optimized geometry of **7** with the obtained crystal structure indicated the suitability of the method (the two structures can be overlaid with a root-

DOI: 10.1021/acs.inorgchem.6b01218
Inorg. Chem. XXXX, XXX, XXX–XXX

Scheme 2. Catalytic Oxygen Evolution Using 3a, 7, or 9 Driven by Sodium Periodate

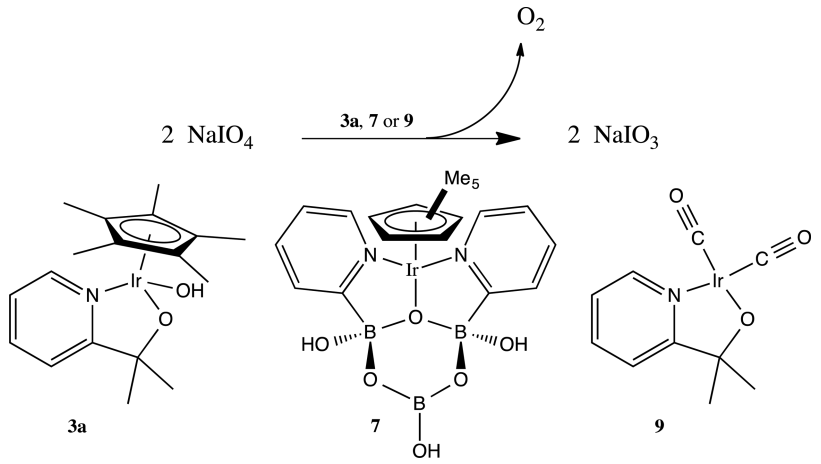

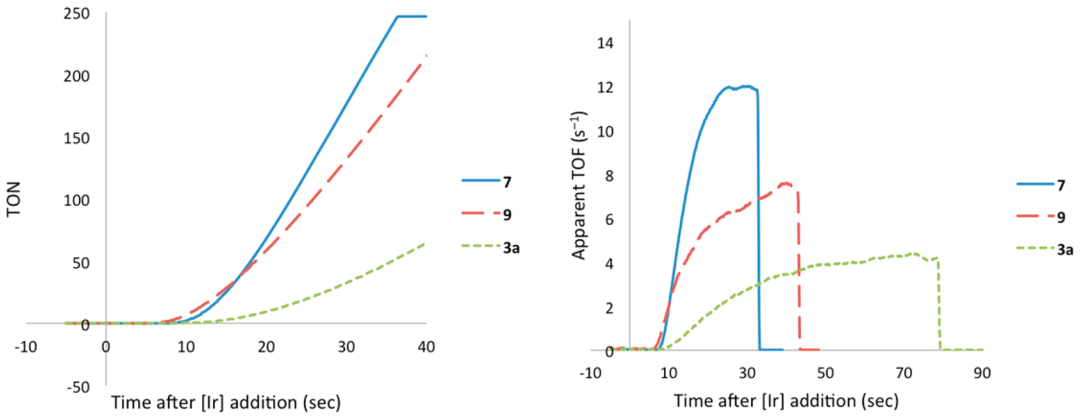

Figure 5. Representative oxygen evolution, as measured by the Clark electrode: TON (left) and TOF (right) comparing 1.0 μM loadings of **3a**, **7**, and **9** in 49.8 mM $NaIO_4$. Saturation of the detector is responsible for the jump discontinuity in TOF curves.

Table 3. Calculated TOF and Induction Period for 1 μM Loadings of 3a, 7, and 9 in 49.8 mM $NaIO_4$, Using a Linear Fit of TON versus Time Data between 15 and 27.5 s after [Ir] Addition

	TOF (s^{-1})		induction period (s)	
[Ir]	average[a]	standard deviation[a]	average[a]	standard deviation[a]
7	10.9	0.7	13.3	0.6
3a	1.9	0.2	14.0	0.7
9	5.8	0.7	11.8	0.4

[a]Average and standard deviation calculated from four trials for each complex.

Table 4. Maximum Observed TOF and Induction Period for 1 μM Loadings of 3a, 7, and 9 in 49.8 mM $NaIO_4$

	maximum TOF (s^{-1})		time elapsed until max TOF (s)	
[Ir]	average[a]	standard deviation[a]	average[a]	standard deviation[a]
7	12.2	1.0	29.2	1.1
3a	4.4	0.1	75.5	2.3
9	7.8	0.6	44.6	4.0

[a]Data from four trials for each compound.

mean-square deviation of only 0.22 Å). Optimizing **7** with six hydrogen-bound water molecules did not substantially change the geometry of the boracycle.

To assess the contribution of d electrons to the bonding interaction between the iridium center and tridentate ligand, the theoretical gas-phase reactions of the hypothetical neutral tridentate ligand (**8**; Table 2) with a series of metal hydroxides were compared. The calculated gas-phase structure of **7** was found to be sufficiently similar to the crystal structure of **7** (vide supra), with a dissociation energy of 65.77 kcal mol^{-1}.

Both group II metals and Cp* complexes of group III metals form complexes that are poor analogues of **7**. The O−M bond is significantly shorter than the N−M bonds, which are also significantly different from each other. It appears that the structure is distorted to bring the metal center closer to one of the hydroxide substituents on the boracycle core. Therefore, it is difficult to compare the energetics with d^0 metals. It should be noted, however, that the calculated dissociation energies for all of these complexes is substantially less than that calculated for **7**, with the exception of the barium complex. In this last case, there is a different binding mode, in which the metal atom is more tightly associated with the oxygen atoms in the exocyclic hydroxide groups (2.67 Å) than to the nitrogen atoms in the pyridyl rings (2.94 Å).

The group XII metals form complexes that resemble the symmetry of **7** much more closely. Of these, the cadmium complex has O−M and N−M bonds that are closest in length to those of **7**. The O−M bond is only 2.9% longer and the N−M bonds only 2.4% longer than those in **7**, but the bond dissociation energy of the cadmium complex is more than 40%

DOI: 10.1021/acs.inorgchem.6b01218
Inorg. Chem. XXXX, XXX, XXX−XXX

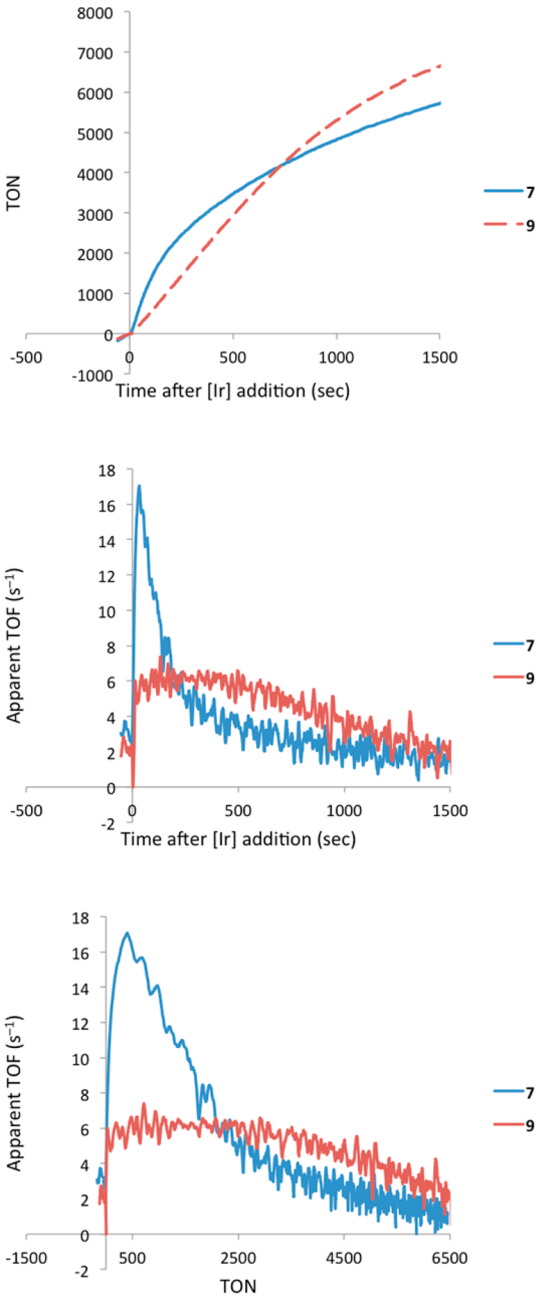

Figure 6. Oxygen evolution data, as measured by the Clark electrode, using10 nM [Ir] in 49.8 mM $NaIO_4$.

smaller than that calculated for **7**. Even in the case of the zinc complex, for which the O−M bond is 9% shorter and the N−M bonds are 7% shorter than the corresponding bonds in **7**, the dissociation energy is still only 22% smaller than that of **7**. The lengths of the B−O bonds in the boracycle appear to be quite insensitive to the identity of the metal, spanning only from 1.46 to 1.52 Å. There may be a slight correlation between the dissociation energy and B−O bond length (R^2 = 54%, excluding barium), but the effect is too small and the trend too weak to support or contradict the hypothesis. Given that the calculated dissociation energy of **7** is substantially greater than that calculated for all d^{10} and d^0 complexes (except barium), it is reasonable to ascribe some of the stability of **7** to a bonding interaction between d electrons on the metal center and electrons in the ligand.

This is supported by computational analysis of the electronic structure of **7**. Depictions of the high-lying occupied frontier molecular orbitals in the calculated structure of **7** indicate a significant interaction between the iridium-centered d orbitals and much of the boracycle core (Figure 4). Examination of the symmetry of the calculated occupied molecular orbitals of **7** indicates the highest occupied molecular orbital (HOMO) to be a largely antibonding interaction between the iridium-centered d_{z^2} orbital and one of the sp^2 orbitals of the adjacent oxygen atom, with some density extending into the rest of the boracycle as well as the Cp* ligand. HOMO−1 appears to be largely a bonding interaction between the iridium-centered d_{xz} orbital and several orbitals in the boracycle. HOMO−2 appears to show the bonding interaction character. While it is difficult to give an accurate estimate of the overall bonding order of that interaction, both the degree of delocalization of these orbitals between the metal center and boracycle and the relatively high dissociation energy compared to the d^0 and d^{10} metals indicate an overall d-electron bonding interaction.

The addition of **7** to a 50 mM solution of CAN resulted in very slow evolution of oxygen, with a measured turnover number (TON) of only 10 in the first 200 s and a maximum observed turnover frequency (TOF) of 0.08 s^{-1} (Figure S17). This rate is more than 250 times slower than that observed under the same conditions but using $NaIO_4$ (vide infra). It is uncertain whether the difference is due to the lower pH of the CAN solution, a different mode of chemical activation, different active species, or a different mechanism of oxygen evolution. Because CAN cannot serve as an oxygen-atom donor, all of this oxygen must have come from the oxidation of water. However, in the case of $NaIO_4$, one or both of the oxygen atoms in a produced O_2 molecule may have originated in the oxidant. Unfortunately, because of extremely rapid exchange, it is not possible to address this question by ^{18}O isotope-labeling studies. Cyclic voltammetry using a boron-doped diamond working electrode in a 0.1 M KNO_3 electrolyte containing 76 μM **7** showed no reversible features and no evidence of electrochemical reaction beyond decomposition of the complex (Figure S18), indicating a substantial difference between $NaIO_4$- and electrode-driven activity.

As with Cp*Ir complexes **1a**, **2a**, and **3a**, **7** was also found to react quickly with sodium periodate to form a highly active periodate-driven oxygen evolution catalyst. Clark electrode quantification of the oxygen evolved from a 49.8 mM $NaIO_4$ solution held at 25.0 °C after the addition of the iridium complex to a final concentration of 1.0 μM [Ir] indicates a TOF greater than 10 s^{-1}, which is significantly faster than those reported for Cp*Ir complexes **1a**, **2a**, and **3a**[1] and faster even than the catalyst formed from $Ir(CO)_2$pyalc (**9**), which was recently reported as one of the most efficient precatalysts.[2] A direct comparison of **7**, **3a**, and **9** under the same experimental conditions (Scheme 2, Figure 5, and Tables 3 and 4) demonstrated this dramatic difference in the TOF.

In each case, the onset of oxygen detection occurred between 10 and 15 s after the addition of the iridium species to the periodate solution. By analysis of the rate of oxygen evolution from 15 s after the addition until 27.5 s after the addition, the initial TOFs were calculated (with 95% confidence error bars) for **7** as 10.9 ± 2.0 s^{-1}, **9** as 5.8 ± 2.1 s^{-1}, and **3a** as 1.9 ± 0.5 s^{-1}. The latter two values are in excellent agreement with the published values.[2] However, if the highest instantaneous TOF during the course of each run is taken as the value, the values increase to 12.2 ± 2.9, 7.8 ± 1.8, and 4.4 ± 0.4 s^{-1}, respectively.

DOI: 10.1021/acs.inorgchem.6b01218
Inorg. Chem. XXXX, XXX, XXX−XXX

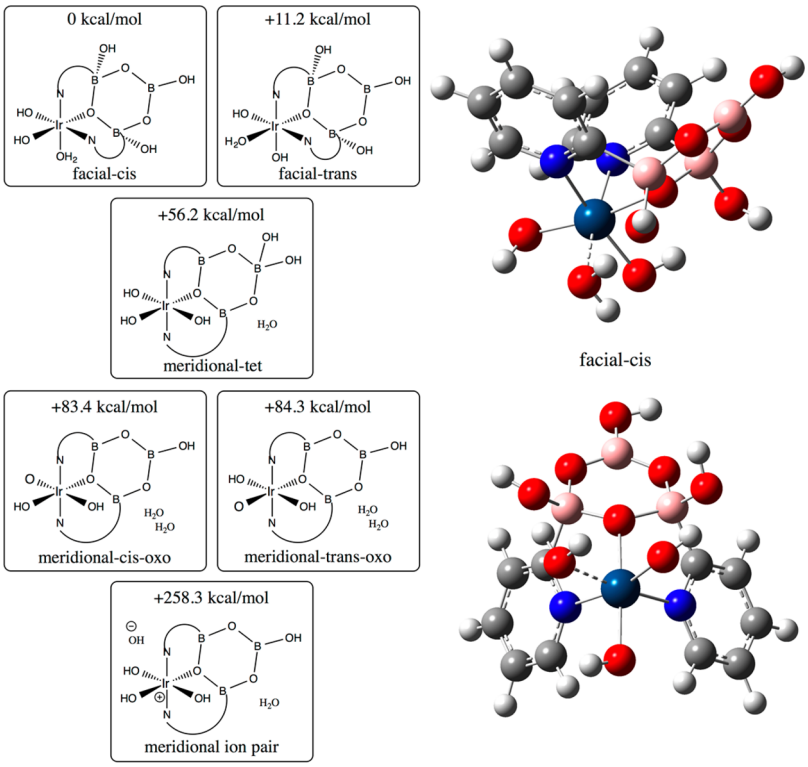

Figure 7. Possible monomeric Ir^{IV}-Dipytribor species with calculated relative enthalpies (left) and two 3D renderings of the most stable isomer, viewed from two different angles (right).

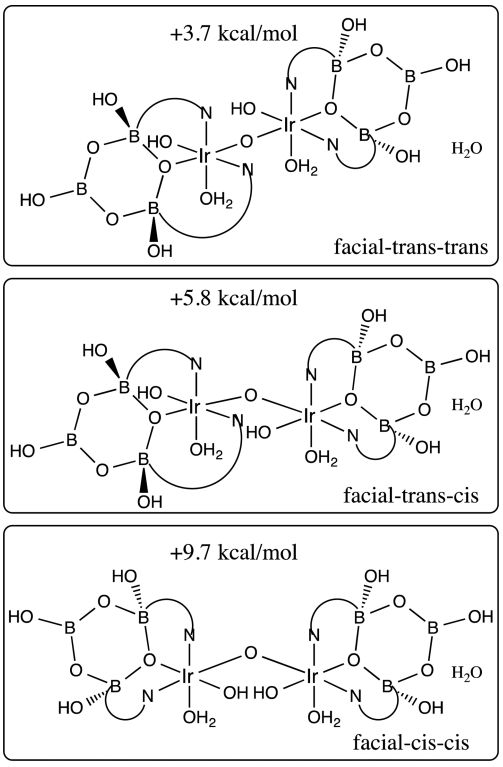

Figure 8. Possible dimeric Ir^{IV}-Dipytribor species with calculated enthalpies relative to the most stable species shown in Figure 7 (2monomer → dimer + H_2O).

The substantial increase in the apparent TOF, especially in the case of **3a**, is indicative of a gradual activation. Modeling the induction period as the *x* intercept of the linear regions of each curve gives similar values for **7** (13.3 ± 1.8 s), **9** (11.8 ± 1.2 s), and **3a** (14.0 ± 2.1 s). However, this is not necessarily a good measure of the activation kinetics for these complexes because mixing is a significant portion of the latency on this time scale. Analysis of the rate of oxygen production (apparent TOF) with respect to time after iridium addition indicates a larger difference in the activation kinetics of the three precatalysts. Oxygen evolution from **7**-catalyzed solutions reaches a maximum rate at approximately 22 s after addition, after which the rate is roughly constant for the next 10 s until the detector is saturated. However, the rate of oxygen evolution from solutions containing **3a** and **9** does not appear to reach a maximum rate before the detector is saturated (ca. 40 s for **9** and ca. 80 s for **3**). That **7** reaches a maximum oxygen evolution rate under these conditions could indicate either that this species is the most quickly activated of the three complexes tested or that it generates an active species that is most quickly deactivated, quickly reaching a momentary steady state for which the activation and deactivation rates are similar.

To remove this ambiguity, oxygen assays were conducted using only 10 nM of either **7** or **9** in 49.8 mM $NaIO_4$, so as to allow probing of the kinetics for longer time periods (Figure 6). Under these conditions, **7** activated quickly, reaching a maximum apparent TOF of 17.1 s^{-1} 32 s after the addition, at which point each iridium atom had turned over an average of 400 times. The apparent TOF then decayed rapidly, returning to within experimental error of the baseline around 1000 s after the addition. In contrast, **9** reached a fairly steady TOF of 5.7 s^{-1} starting 11 s after the addition and continuing for about 800 s (standard deviation of 0.6 s^{-1} over this period), after which there was a steady decline in the rate of oxygen evolution, returning to within experimental error of the baseline around 1500 s after the addition.

DOI: 10.1021/acs.inorgchem.6b01218
Inorg. Chem. XXXX, XXX, XXX−XXX

After oxygen evolution had ceased, the pH of the solution was found to have fallen to 4.0 from a starting pH of 5.1. ^{1}H NMR spectroscopy suggested complete conversion of the Cp* ring into acetate, which is consistent with previous findings,[1−3] and the production of multiple pyridyl-containing species (Figure S14). ^{11}B NMR spectroscopy indicated only one species, with a chemical shift of 19.3 ppm, consistent with boric acid (Figure S15). The resulting solution had a single strong absorbance in the visible region, λ_{max} = 580 nm, which could be consistent with either hydrated iridium oxide nanoparticles or molecular iridium(IV)−iridium(IV) dimeric species.[2,3] Real-time dynamic light scattering (DLS) measurements indicated no formation of nanoparticles within 1 h of the addition of **7** to a 50 mM $NaIO_4$ solution at loadings between 100 nm and 2.0 μM. However, nanoparticles were evident by 4 h after the addition. Together these DLS and UV−vis measurements are consistent with a final species similar to that generated by the oxidation of $(Cp^*Ir)_2(OH)_4$ by $NaIO_4$.[3] At this point, however, it appears that the catalytically active species during the first 60 s of oxygen evolution is likely molecular.

Because the catalytically active species generated by reaction with $NaIO_4$ is too short-lived to be well-characterized experimentally and appears to be molecular, several plausible binding modes of the Dipytribor ligand with an octahedral iridium(IV) center were examined computationally. In the absence of conclusive experimental structural data, it is not possible to determine the speciation of catalytically active compounds derived from **7**. However, candidate structures can be proposed by analogy to those studied in previously published systems, and computed relative enthalpies of formation offer a way to compare the likelihood of these proposed structures existing under the reaction conditions.

It is known that periodate-mediated activation of complexes **1a**, **2a**, and **3a** proceeds with rapid conversion of the Cp* moiety to acetate,[1−3] and this appears to be the case as well for the oxidation of **7** with periodate. It has been shown[6,54] that in aqueous solution, Cp*Ir complexes such as **3a** and Cp*Ir(pyridine)Cl_2, with weakly bound ligands, are in equilibrium with $Cp^*Ir(OH_2)_3^{2+}$, which is known[4] to form iridium-containing nanoparticles very quickly under the action of $NaIO_4$. In contrast, complexes such as **1a**, **2a**, and **3a** retain their strongly bound bidentate ligands and remain homogeneous under the action of $NaIO_4$.[4] Because rapid particle formation is not observed in the case of **7**, it is reasonable to assume that some polydentate ligand remains bound to the iridium center during oxygen evolution.

Without the Cp* ligand enforcing a tetrahedral coordination sphere about iridium, the tridentate ligand has the opportunity to adopt either a planar, meridional, pincer-type binding mode, ejecting the exocyclic hydroxide substituents from the boracycle or remaining as a scorpionate ligand, binding in a facial configuration. Gas-phase calculations comparing the stability of possible isomers of hydrated iridium(IV) hydroxo species reveal a very strong preference (>45 kcal mol^{-1}) for the scorpionate binding mode (Figure 7). The favored scoprionate facial chelation mode differentiates this ligand from the meridional-specific ligands, like terpyridine.

Because mono(μ-oxo) dimeric specieis have recently been implicated as possible catalytically active species,[55,56] three likely mono(μ-oxo) dimers of the most stable monomeric species were also modeled computationally (Figure 8). When accounting for the enthalpy of formation of the dissociated water, the enthalpies of formation of these dimeric species are only slightly less favorable than the most stable monomeric species. Therefore, we cannot rule out the possibility of these species existing under experimental conditions.

CONCLUSIONS

An iridium complex (**7**) of a tridentate, mixed organic−inorganic ligand was prepared from **6**. Both **6** and **7** were found to be surprisingly hydrolytically stable in aqueous solution for days and weeks (respectively) at 23 °C. The unique boracycle at the core of the tridentate ligand binds to iridium through an endocyclic oxygen atom, but the whole ring appears to have a significant covalent bonding interaction with the d orbitals on the iridium center. Complex **7** is a fast-activating precatalyst for a chemically driven oxygen evolution catalyst with a TOF of at least 15 s^{-1} in a solution of 50 mM sodium periodate at 25.0 °C. However, this activity is short-lived, ceasing almost entirely within 5 min under these conditions. The nature of the catalytically active species and mechanism of oxygen formation are currently the subjects of further study.

ASSOCIATED CONTENT

Supporting Information

The Supporting Information is available free of charge on the ACS Publications website at DOI: 10.1021/acs.inorgchem.6b01218.

Experimental and theoretical methods, spectroscopic and crystallographic data, and measured and calculated atomic coordinates (PDF)

X-ray crystallographic data in CIF format (CIF)

AUTHOR INFORMATION

Corresponding Author

*E-mail: robert.crabtree@yale.edu.

Author Contributions

The manuscript was written through contributions of all authors. All authors have given approval to the final version of the manuscript.

Notes

The authors declare no competing financial interest.

ACKNOWLEDGMENTS

This work was funded by a generous donation from the TomKat Charitable Trust and also supported as part of the Argonne−Northwestern Solar Energy Research (ANSER) Center, an Energy Frontier Research Center, funded by the U.S. Department of Energy, Office of Science, Office of Basic Energy Sciences, under Awards DE-PS02-08ER15944 and DE-SC0001059 (V.S.B. and R.H.C.). DLS measurements were carried out in the Facility for Light Scattering at Yale University. We thank Catalytic Innovations LLC for the generous gift of **3a** and Daria Huang for the generous gift of **9**.

REFERENCES

(1) Hintermair, U.; Sheehan, S. W.; Parent, A. R.; Ess, D. H.; Richens, D. AT.; Vaccaro, P. H.; Brudvig, G. W.; Crabtree, R. H. *J. Am. Chem. Soc.* **2013**, *135*, 10837.

(2) Huang, D. L.; Beltrán-Suito, R.; Thomsen, J. M.; Hashmi, S. M.; Materna, K. L.; Sheehan, S. W.; Mercado, B. Q.; Brudvig, G. W.; Crabtree, R. H. *Inorg. Chem.* **2016**, *55*, 2427.

(3) Parent, A. R.; Brewster, T. P.; De Wolf, W.; Crabtree, R. H.; Brudvig, G. W. *Inorg. Chem.* **2012**, *51*, 6147.

DOI: 10.1021/acs.inorgchem.6b01218
Inorg. Chem. XXXX, XXX, XXX−XXX

(4) Hintermair, U.; Hashmi, S. M.; Elimelech, M.; Crabtree, R. H. *J. Am. Chem. Soc.* **2012**, *134*, 9785.
(5) Thomsen, J. M.; Sheehan, S. W.; Hashmi, S. M.; Campos, J.; Hintermair, U.; Crabtree, R. H.; Brudvig, G. W. *J. Am. Chem. Soc.* **2014**, *136*, 13826.
(6) Koelewijn, J. M.; Lutz, M.; Dzik, W. I.; Detz, R. J.; Reek, J. N. H. *ACS Catal.* **2016**, *6*, 3418−3427.
(7) Zuccaccia, C.; Bellachioma, G.; Bortolini, O.; Bucci, A.; Savini, A.; Macchioni, A. *Chem. - Eur. J.* **2014**, *20*, 3446−3456.
(8) Petronilho, A.; Llobet, A.; Albrecht, M. *Inorg. Chem.* **2014**, *53*, 12896−12901.
(9) Grotjahn, D. B.; Brown, D. B.; Martin, J. K.; Marelius, D. C.; Abadjian, M.-C.; Tran, H. N.; Kalyuzhny, G.; Vecchio, K. S.; Specht, Z. G.; Cortes-Llamas, S. A.; Miranda-Soto, V.; van Niekerk, C.; Moore, C. E.; Rheingold, A. L. *J. Am. Chem. Soc.* **2011**, *133*, 19024−19027.
(10) Savini, A.; Bucci, A.; Bellachioma, G.; Giancola, S.; Palomba, F.; Rocchigiani, L.; Rossi, A.; Suriani, M.; Zuccaccia, C.; Macchioni, A. *J. Organomet. Chem.* **2014**, *771*, 24−32.
(11) Ingram, A. J.; Wolk, A. B.; Flender, C.; Zhang, J.; Johnson, C. J.; Hintermair, U.; Crabtree, R. H.; Johnson, M. A.; Zare, R. N. *Inorg. Chem.* **2014**, *53*, 423.
(12) Heiden, Z. M.; Rauchfuss, T. B. *J. Am. Chem. Soc.* **2007**, *129*, 14303−14310.
(13) Zhou, M.; Schley, N. D.; Crabtree, R. H. *J. Am. Chem. Soc.* **2010**, *132*, 12550.
(14) Zhou, M.; Balcells, D.; Parent, A. R.; Crabtree, R. H.; Eisenstein, O. *ACS Catal.* **2012**, *2*, 208.
(15) Zhou, M.; Hintermair, U.; Hashiguchi, B. G.; Parent, A. R.; Hashmi, S. M.; Elimelech, M.; Periana, R. A.; Brudvig, G. W.; Crabtree, R. H. *Organometallics* **2013**, *32*, 957.
(16) Xu, C.; Goh, L. Y.; Pullarkat, S. A. *Organometallics* **2011**, *30*, 6499−6502.
(17) Springsteen, G.; Wang, B. *Tetrahedron* **2002**, *58*, 5291−5300.
(18) Fischer, F. C.; Havinga, E. *Recl. Trav. Chim. Pays-Bas* **1974**, *93*, 21−24.
(19) Tyrrell, E.; Brookes, P. *Synthesis* **2004**, *4*, 469−483.
(20) Chen, K.; Peterson, R.; Math, S. K.; LaMunyon, J. B.; Testa, C. A.; Cefalo, D. R. *Tetrahedron Lett.* **2012**, *53*, 4873−4876.
(21) Nishihara, Y.; Nara, K.; Osakada, K. *Inorg. Chem.* **2002**, *41*, 4090−4092.
(22) Nishihara, Y.; Nara, K.; Nishide, Y.; Osakada, K. *Dalton Trans.* **2004**, 1366.
(23) Itazaki, M.; Nishihara, Y.; Osakada, K. *Organometallics* **2004**, *23*, 1610−1621.
(24) Möhlmann, L.; Wendt, O. F.; Johnson, M. T. *Acta Crystallogr., Sect. E: Struct. Rep. Online* **2011**, *67*, m719−m720.
(25) Nielsen, D. K.; Doyle, A. G. *Angew. Chem., Int. Ed.* **2011**, *50*, 6056.
(26) Sung, H. H.-Y.; Wu, M. W.; Williams, I. D. *Inorg. Chem. Commun.* **2000**, *3*, 401.
(27) Lan, S.-M.; Di, W.-J.; Shao, Z.-D.; Liang, Y.-X. *Acta Crystallogr., Sect. C: Cryst. Struct. Commun.* **2011**, *67*, m338−m341.
(28) Zhang, H.-X.; Zheng, S.-T.; Yang, G.-Y. *Acta Crystallogr., Sect. C: Cryst. Struct. Commun.* **2004**, *60*, m241−m243.
(29) Yang, Y.; Wang, Y.; Sun, J.; Cui, M.; Meng, C. *Z. Anorg. Allg. Chem.* **2011**, *637*, 729.
(30) Wang, G.-M.; Li, J.-H.; Li, Z.-X.; Wang, P.; Li, H. *Z. Anorg. Allg. Chem.* **2008**, *634*, 1192.
(31) Dostál, L.; Jambor, R.; Růžička, A.; Jirasko, R.; Lyčka, A.; Beckmann, J.; Ketkov, S. *Inorg. Chem.* **2015**, *54*, 6010−6019.
(32) Kliegel, W.; Drückler, K.; Patrick, B. O.; Rettig, S. J.; Trotter, J. *Acta Crystallogr., Sect. E: Struct. Rep. Online* **2002**, *58*, o831−o833.
(33) Beckett, M. A.; Coles, S. J.; Light, M. E.; Fischer, L.; Stiefvater-Thomas, B. M.; Varma, K. S. *Polyhedron* **2006**, *25*, 1011.
(34) Beckett, M. A.; Horton, P. N.; Hursthouse, M. B.; Timmis, J. L. *RSC Adv.* **2013**, *3*, 15185.
(35) Trofimenko, S. *Polyhedron* **2004**, *23*, 197.
(36) Paulo, A.; Correia, J. D. G.; Campello, M. P. C.; Santos, I. *Polyhedron* **2004**, *23*, 331.
(37) Reglinski, J.; Spicer, M. D. *Coord. Chem. Rev.* **2015**, *297*−*298*, 181.
(38) Hill, A. F.; Owen, G. R.; White, A. J. P.; Williams, D. J. *Angew. Chem., Int. Ed.* **1999**, *38*, 2759.
(39) Spicer, M. D.; Reglinski, J. *Eur. J. Inorg. Chem.* **2009**, *2009*, 1553.
(40) Braunschweig, H.; Dewhurst, R. D.; Schneider, A. *Chem. Rev.* **2010**, *110*, 3924.
(41) Hill, A. F.; Lee, S. B.; Park, J.; Shang, R.; Willis, A. C. *Organometallics* **2010**, *29*, 5661.
(42) Pettinari, R.; Pettinari, C.; Marchetti, F.; Monari, M.; Mosconi, E.; De Angelis, F. *Organometallics* **2013**, *32*, 3895−3902.
(43) Tönnemann, J.; Risse, J.; Grote, Z.; Scopelliti, R.; Severin, K. *Eur. J. Inorg. Chem.* **2013**, *2013*, 4558.
(44) *CrysAlisPro*; Rigaku OD: The Woodlands, TX, 2015.
(45) Sheldrick, G. M. *Acta Crystallogr., Sect. A: Found. Crystallogr.* **2008**, *64*, 112.
(46) Dorta, R.; Broggini, D.; Kissner, R.; Togni, A. *Chem. - Eur. J.* **2004**, *10*, 4546.
(47) Dorta, R.; Broggini, D.; Stoop, R.; Rüegger, H.; Spindler, F.; Togni, A. *Chem. - Eur. J.* **2004**, *10*, 267.
(48) Sieh, D.; Schlimm, M.; Andernach, L.; Angersbach, F.; Nückel, S.; Schöffel, J.; Šušnjar, N.; Burger, P. *Eur. J. Inorg. Chem.* **2012**, *2012*, 444.
(49) Tokunaga, Y. *Heterocycles* **2013**, *87*, 991.
(50) Marinaro, W. A.; Schieber, L. J.; Munson, E. J.; Day, V. W.; Stella, V. J. *J. Pharm. Sci.* **2012**, *101*, 3190.
(51) Zhang, A.-Y.; Yao, Y.; Li, L.-J.; Song, P.-S. *J. Chem. Thermodyn.* **2005**, *37*, 101.
(52) Salentine, C. G. *Inorg. Chem.* **1983**, *22*, 3920−3924.
(53) Kohn, W.; Sham, L. J. *Phys. Rev.* **1965**, *140*, A1133.
(54) Cayemittes, S.; Poth, T.; Fernandez, M. J.; Lye, P. G.; Becker, M.; Elias, H.; Merbach, A. E. *Inorg. Chem.* **1999**, *38*, 4309−4316.
(55) López, I.; Ertem, M. Z.; Maji, S.; Benet-Buchholz, J.; Keidel, A.; Kuhlmann, U.; Hildebrandt, P.; Cramer, C. J.; Batista, V. S.; Llobet, A. *Angew. Chem., Int. Ed.* **2014**, *53*, 205−209.
(56) Yang, K. R.; Matula, A. J.; Kwon, G.; Hong, J.; Sheehan, S. W.; Thomsen, J. M.; Brudvig, G. W.; Crabtree, R. H.; Tiede, D. M.; Chen, L. X.; Batista, V. S. *J. Am. Chem. Soc.* **2016**, *138*, 5511−5514.

DOI: 10.1021/acs.inorgchem.6b01218
Inorg. Chem. XXXX, XXX, XXX−XXX